

Photoinduced Infrared Absorption of Quasi-One-Dimensional Halogen-Bridged Binuclear Transition-Metal Complexes

Jun Ohara and Shoji Yamamoto

Division of Physics, Hokkaido University, Sapporo 060-0810, Japan

(Dated: November 26, 2018)

We investigate the optical conductivity of photogenerated solitons in quasi-one-dimensional halogen-bridged binuclear transition-metal (*MMX*) complexes with particular emphasis on a comparison among the three distinct groups: $A_4[\text{Pt}_2(\text{P}_2\text{O}_5\text{H}_2)_4X]\cdot n\text{H}_2\text{O}$ ($X = \text{Cl, Br, I}$; $A = \text{Na, K, NH}_4, \dots$), $\text{Pt}_2(\text{RCS}_2)_4\text{I}$ ($R = \text{C}_n\text{H}_{2n+1}$) and $\text{Ni}_2(\text{CH}_3\text{CS}_2)_4\text{I}$, which exhibit a mixed-valent ground state with the X sublattice dimerized, that with the M_2 sublattice dimerized and a Mott-Hubbard magnetic ground state, respectively. Soliton-induced absorption spectra for $A_4[\text{Pt}_2(\text{P}_2\text{O}_5\text{H}_2)_4X]\cdot n\text{H}_2\text{O}$ should split into two bands, while that for $\text{Pt}_2(\text{RCS}_2)_4\text{I}$ and $\text{Ni}_2(\text{CH}_3\text{CS}_2)_4\text{I}$ should consist of a single band. The excitonic effect is significant in $\text{Ni}_2(\text{CH}_3\text{CS}_2)_4\text{I}$.

PACS numbers: PACS numbers: 71.45.Lr, 42.65.Tg, 78.20.Ci, 78.20.Bh

MX chains, that is, a family of quasi-one-dimensional halogen (X)-bridged transition-metal (M) complexes, provide an exciting stage¹⁻⁴ performed by electron-electron correlation, electron-lattice interaction, low dimensionality and d - p orbital hybridization. In recent years, binuclear metal analogs which are referred to as *MMX* chains have stimulated renewed interest^{5,6} in this system. The existent *MMX* compounds consist of three groups: $A_4[\text{Pt}_2(\text{pop})_4X]\cdot n\text{H}_2\text{O}$ ($X = \text{Cl, Br, I}$; $A = \text{Li, Cs, } \dots$; $\text{pop} = \text{diphosphonate} = \text{P}_2\text{O}_5\text{H}_2^{2-}$)^{7,8}, $\text{Pt}_2(\text{RCS}_2)_4\text{I}$ ($R = \text{alkyl chain} = \text{C}_n\text{H}_{2n+1}$)^{9,10} and $\text{Ni}_2(\text{dta})_4\text{I}$ ($\text{dta} = \text{dithioacetate} = \text{CH}_3\text{CS}_2^-$)¹¹. $A_4[\text{Pt}_2(\text{pop})_4X]\cdot n\text{H}_2\text{O}$ resembles conventional *MX* compounds and generally exhibits a similar ground state of mixed valence with halogen-sublattice dimerization^{12,13}, which is referred to as the charge-density-wave (CDW) state. $\text{Pt}_2(\text{RCS}_2)_4\text{I}$ exhibits a distinct ground state with metal-sublattice dimerization¹⁴, which is referred to as the alternate charge-polarization (ACP) state. $\text{Ni}_2(\text{dta})_4\text{I}$ exhibits the averaged-valence state without any lattice distortion¹⁵ and is regarded as an insulator of the Mott-Hubbard (MH) type. These ground states can be tuned by pressure¹⁶⁻¹⁹ as well as replacing the bridging halogens^{13,20}, counter ions^{18,21} and ligand molecules²².

In such circumstances, topological excitations²³ such as solitons and polarons have been found for an *MMX* Hamiltonian of the Su-Schrieffer-Heeger type²⁴ and an analogy between *MMX* chains and *trans*-polyacetylene has been pointed out. The direct $M(d_{z^2})$ - $M(d_{z^2})$ overlap effectively reduces the on-site Coulomb repulsion and therefore electrons can be more itinerant in *MMX* chains. In fact *MMX* chains exhibit much higher room-temperature conductivity than *MX* chains¹⁴. Solitons generally have lower formation energies and smaller effective masses than polarons in *MMX* chains²⁵. Then we take more and more interest in *MMX* solitons as charge or spin carriers. While *MMX* uniform absorption spectra have recently been investigated²⁶, but photoinduced ones, which serve as prominent probes for nonlinear excitations, have neither measured nor calculated yet. Thus

motivated, we study optical conductivity for *MMX* solitons and illuminate a possible contrast among the family compounds.

We describe *MMX* chains by the one-dimensional $\frac{3}{4}$ -filled single-band Peierls-Hubbard Hamiltonian

$$\begin{aligned} \mathcal{H} = & - \sum_{n,s} \left\{ t_{MM} b_{n,s}^\dagger a_{n,s} + [t_{MXM} \right. \\ & \left. - \alpha(v_{n+1} - v_n)] a_{n+1,s}^\dagger b_{n,s} + \text{H.c.} \right\} \\ & - \beta \sum_{n,s} [(v_n - u_{n-1})n_{n,s} + (u_n - v_n)m_{n,s}] \\ & + U_M \sum_n (n_{n,+}n_{n,-} + m_{n,+}m_{n,-}) \\ & + \sum_{n,s,s'} (V_{MM}n_{n,s}m_{n,s'} + V_{MXM}n_{n+1,s}m_{n,s'}) \\ & + \frac{K_{MX}}{2} \sum_n [(u_n - v_n)^2 + (v_n - u_{n-1})^2], \quad (1) \end{aligned}$$

where $n_{n,s} = a_{n,s}^\dagger a_{n,s}$ and $m_{n,s} = b_{n,s}^\dagger b_{n,s}$ with $a_{n,s}^\dagger$ and $b_{n,s}^\dagger$ being the creation operators of an electron with spin $s = \pm$ (up and down) for the $M d_{z^2}$ orbitals in the n th *MMX* unit. t_{MM} and t_{MXM} describe the intradimer and interdimer electron hoppings, respectively. α and β are the intersite and intrasite electron-lattice coupling constants, respectively, with K_{MX} being the metal-halogen spring constant. u_n and v_n are, respectively, the chain-direction displacements of the halogen and metal dimer in the n th *MMX* unit from their equilibrium positions. We assume, based on the thus-far reported experimental observations, that every M_2 moiety is not deformed. The lattice distortion is adiabatically determined through the Hellmann-Feynman force equilibrium condition. We show in Fig. 1 the ground-state phase diagrams within the Hartree-Fock (HF) approximation. Setting t_{MXM} and K_{MX} both equal to unity, we adopt a common parameter set: $t_{MM} = 2.0$, $V_{MM} = 0.5$, $V_{MXM} = 0.3$. The rest are taken in three ways as a) $U_M = 1.0$, $\alpha = 0.0$, $\beta = 1.4$; b) $U_M = 1.0$, $\alpha = 0.3$, $\beta =$

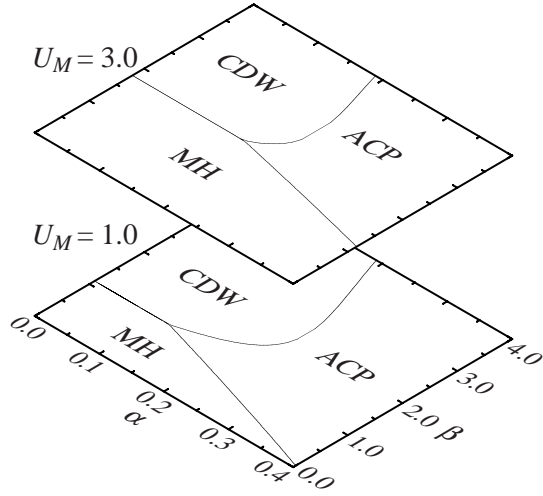


FIG. 1: Ground-state phase diagrams.

1.0; c) $U_M = 3.0, \alpha = 0.3, \beta = 1.0$; which are relevant to $A_4[\text{Pt}_2(\text{pop})_4X] \cdot n\text{H}_2\text{O}$, $\text{Pt}_2(\text{RCS}_2)_4\text{I}$ and $\text{Ni}_2(\text{dta})_4\text{I}$, and indeed give the CDW, ACP and MH ground states, respectively.

The optical spectra are obtained by calculating the matrix elements between the ground state $|g\rangle$ of energy E_g and the excited states $|l\rangle$ of energy E_l ($l = 1, 2, \dots$) for the current operator

$$\begin{aligned} \mathcal{J} = & \frac{ie}{\hbar} \sum_{n=1}^N \sum_{s=\pm} \left\{ c_{MM} t_{MM} (b_{n,s}^\dagger a_{n,s} - a_{n,s}^\dagger b_{n,s}) \right. \\ & + c_{MXM} [t_{MXM} - \alpha(v_{n+1} - v_n)] \\ & \left. \times (a_{n+1,s}^\dagger b_{n,s} - b_{n,s}^\dagger a_{n+1,s}) \right\}, \end{aligned} \quad (2)$$

where c_{MM} and c_{MXM} are the average M - M and M - X - M distances, respectively, and are set for $c_{MXM} = 2c_{MM}$. The real part of the optical conductivity is given by

$$\sigma(\omega) = \frac{\pi}{N\omega} \sum_l |\langle l | \mathcal{J} | g \rangle|^2 \delta(E_l - E_g - \hbar\omega). \quad (3)$$

$|g\rangle$ is set for the HF ground state, while $|l\rangle$ is calculated within and beyond the HF approximation, being generally defined as

$$|l\rangle = \sum_s \sum_{\epsilon_\mu \leq \epsilon_F} \sum_{\epsilon_\nu > \epsilon_F} f(\mu, \nu, s; l) c_{\nu,s}^\dagger c_{\mu,s} |g\rangle, \quad (4)$$

where ϵ_F is the Fermi energy and $c_{\lambda,s}^\dagger$ creates an electron with spin s for the λ th HF eigenstate with an eigenvalue ϵ_λ . In the HF scheme, any excited state is simply approximated by a single Slater determinant as $f(\mu, \nu, s; l) = \delta_{\mu\nu s, l}$. We further consider excited states of the configuration-interaction (CI) type, where $f(\mu, \nu, s; l)$ is determined so as to diagonalize the original Hamiltonian (1). We set N equal to 84, where 2 GB memory is necessary for the CI calculation.

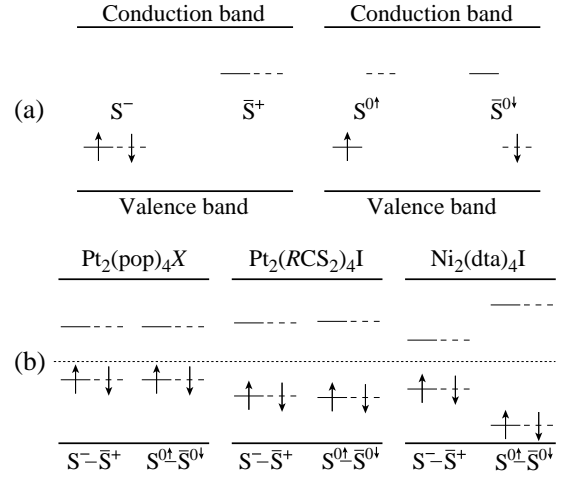


FIG. 2: Localized levels due to solitons in a pair, where the solid and broken segments designate those for up-spin (\uparrow) and down-spin (\downarrow) electrons, respectively. (a) Qualitative illustrations for charged and neutral soliton pairs. (b) Quantitative illustrations for soliton pairs in $A_4[\text{Pt}_2(\text{pop})_4X] \cdot n\text{H}_2\text{O}$, $\text{Pt}_2(\text{RCS}_2)_4\text{I}$ and $\text{Ni}_2(\text{dta})_4\text{I}$, where the dotted line designates the center of the gap.

Since photogenerated defects are necessarily in pairs, we find the most stable soliton (S)-antisoliton (\bar{S}) pair at a sufficiently low temperature $k_B T / t_{MXM} = 10^{-3}$ without any assumption on the soliton shapes. A pair of solitons generally gives two additional levels within the gap, as is illustrated in Fig. 2(a). There appear further soliton-related intragap levels in the strong-coupling region²⁷. These levels are strongly localized and completely assigned to each soliton. The spin up-down symmetry holds with a charged soliton pair $S^- - \bar{S}^+$, whereas it breaks down with a neutral soliton pair $S^{0\uparrow} - \bar{S}^{0\downarrow}$. The lower level is doubly filled, while the upper one is vacant. Considering that there is no essential overlap between the wave functions of well-separated S and \bar{S} , either an optical transition between the vacant soliton level and the valence band or that between the filled soliton level and the conduction band may yield absorption in the gap. The level structure of any soliton pair quantitatively depends on the background compound and typical energy schemes are predicted in Fig. 2(b). Since the electron-hole symmetry is broken in the Hamiltonian (1), soliton-related electron and hole levels may be asymmetric with respect to the center of the gap. It is indeed the case with the CDW background of $A_4[\text{Pt}_2(\text{pop})_4X] \cdot n\text{H}_2\text{O}$, whereas on the ACP background of $\text{Pt}_2(\text{RCS}_2)_4\text{I}$ and the MH background of $\text{Ni}_2(\text{dta})_4\text{I}$, a soliton of charge σ , S^σ , and that of spin s , S^{0s} , described in terms of electrons are still nearly equivalent to their counterparts $S^{-\sigma}$ and S^{0-s} described in terms of holes, respectively.

In consequence, *photoinduced soliton absorption spectra for $A_4[\text{Pt}_2(\text{pop})_4X] \cdot n\text{H}_2\text{O}$ should split into two bands, while those for $\text{Pt}_2(\text{RCS}_2)_4\text{I}$ and $\text{Ni}_2(\text{dta})_4\text{I}$ should*

FIG. 3: Hartree-Fock (HF) and single-excitation configuration-interaction (SECI) calculations of the optical conductivity spectra for the optimum soliton-antisoliton pairs on the CDW, ACP and MH backgrounds, where each line has been Lorentzian-broadened. The mid-gap absorption bands due to solitons are scaled up in insets.

consist of a single band, as is demonstrated in Fig. 3. The excitonic effect is remarkable in the strong-correlation compound $\text{Ni}_2(\text{dta})_4\text{I}$. In mixed-valent MX chains, neutral solitons seem to be the lowest-energy pair excitations^{28,29}. In mixed-valent MMX chains, on the other hand, charged solitons may be the lowest-energy excitations because the on-site Coulomb repulsion U_M and the Holstein coupling β are effectively smaller and larger, respectively^{6,14}. Polarons have much higher formation energies for both MX ^{2,28} and MMX ²⁵ chains and can therefore be generated from relatively high-energy excited states corresponding to the electron-hole continuum³⁰. An excitation energy close to the Peierls gap directly induces charge-transfer excitons³¹ and they may relax into soliton pairs for MMX chains as well. The optical conductivity spectra for $A_4[\text{Pt}_2(\text{pop})_4X] \cdot n\text{H}_2\text{O}$ clearly distinguish between charged and neutral solitons. The charged (neutral)-soliton mid-gap absorption spec-

trum is double-peaked and the higher (lower)-energy band has larger oscillator strength. As for $\text{Pt}_2(\text{dta})_4\text{I}$ and $\text{Ni}_2(\text{dta})_4\text{I}$, further measurements such as electron spin resonance³² are supplementary to find out which kind of solitons.

Besides the optimum soliton solutions, there are some metastable ones in general^{25,33}. In $\text{Ni}_2(\text{dta})_4\text{I}$, their energy difference is relatively large and therefore the absorption spectra may significantly vary with the soliton type. Photoinduced infrared absorption measurements on MMX compounds must provide rich physics and are thus encouraged.

The authors are grateful to K. Iwano, Y. Shimoi and H. Okamoto for fruitful discussions and helpful comments. This work was supported by the Ministry of Education, Culture, Sports, Science and Technology of Japan and the Iketani Science and Technology Foundation.

¹ K. Nasu, J. Phys. Soc. Jpn. **52** (1983) 3865.

² J. T. Gammel, A. Saxena, I. Batistić, A. R. Bishop, S. R. Phillpot, Phys. Rev. B **45** (1992) 6408.

³ S. W. Weber-Milbrodt, J. T. Gammel, A. R. Bishop, E. Y. Loh, Jr., Phys. Rev. B **45** (1992) 6435.

⁴ S. Yamamoto, Phys. Lett. A **247** (1998) 422.

⁵ M. Kuwabara, K. Yonemitsu, Mol. Cryst. Liq. Cryst. **341** (2000) 533.

⁶ S. Yamamoto, Phys. Rev. B **63** (2001) 125124.

⁷ C.-M. Che, F. H. Herbstein, W. P. Schaefer, R. E. Marsh, H. B. Gray, J. Am. Chem. Soc. **105** (1983) 4604.

⁸ R. J. H. Clark, M. Kurmoo, H. M. Dawes, M. B. Hursthouse, Inorg. Chem. **25** (1986) 409.

⁹ C. Bellitto, A. Flamini, L. Gastaldi, L. Scaramuzza, Inorg.

Chem. **22** (1983) 444.

¹⁰ S. Ikeuchi, K. Saito, Y. Nakazawa, A. Sato, M. Mitsumi, K. Toriumi, M. Sorai, Phys. Rev. B **66** (2002) 115110.

¹¹ C. Bellitto, G. Dessy, V. Fares, Inorg. Chem. **24** (1985) 2815.

¹² N. Kimura, H. Ohki, R. Ikeda, M. Yamashita, Chem. Phys. Lett. **220** (1994) 40.

¹³ L. G. Butler, M. H. Zietlow, C.-M. Che, W. P. Schaefer, S. Sridhar, P. J. Grunthaner, B. I. Swanson, R. J. H. Clark, H. B. Gray, J. Am. Chem. Soc. **110** (1988) 1155.

¹⁴ H. Kitagawa, N. Onodera, T. Sonoyama, M. Yamamoto, T. Fukawa, T. Mitani, M. Seto, Y. Maeda, J. Am. Chem. Soc. **121** (1999) 10068.

- ¹⁵ I. Shirotani, A. Kawamura, M. Yamashita, K. Toriumi, H. Kawamura, T. Yagi, *Synth. Met.* **64** (1994) 265.
- ¹⁶ M. A. Stroud, H. G. Drickamer, M. H. Zietlow, H. B. Gray, B. I. Swanson, *J. Am. Chem. Soc.* **111** (1989) 66.
- ¹⁷ S. Yamamoto, *Phys. Rev. B* **64** (2001) 140102(R).
- ¹⁸ H. Matsuzaki, T. Matsuka, H. Kishida, K. Takizawa, H. Miyasaka, K. Sugiura, M. Yamashita, H. Okamoto, *Phys. Rev. Lett.* **90** (2003) 046401.
- ¹⁹ H. Ito, Y. Hasegawa, H. Tanaka, S. Kuroda, M. Mitsumi, K. Toriumi, *J. Phys. Soc. Jpn.* **72** (2003) 2149.
- ²⁰ S. Yamamoto, *J. Phys. Soc. Jpn.* **70** (2001) 1198.
- ²¹ M. Yamashita, S. Miya, T. Kawashima, T. Manabe, T. Sonoyama, H. Kitagawa, T. Mitani, H. Okamoto, R. Ikeda, *J. Am. Chem. Soc.* **121** (1999) 2321.
- ²² S. Ikeuchi, K. Saito, Y. Nakazawa, M. Mitsumi, K. Toriumi, M. Sorai, *J. Phys. Chem. B* **108** (2004) 387.
- ²³ S. Yamamoto, M. Ichioka, *J. Phys. Soc. Jpn.* **71** (2002) 189.
- ²⁴ W. P. Su, J. R. Schrieffer, A. J. Heeger, *Phys. Rev. Lett.* **428** (1979) 1698.
- ²⁵ S. Yamamoto, *Phys. Rev. B* **66** (2002) 165113.
- ²⁶ M. Kuwabara, K. Yonemitsu, *J. Mater. Chem.* **11** (2001) 2163.
- ²⁷ Y. Tagawa, N. Suzuki, *J. Phys. Soc. Jpn.* **59** (1990) 4074.
- ²⁸ K. Iwano, *J. Phys. Soc. Jpn.* **66** (1997) 1088.
- ²⁹ J. Ohara, S. Yamamoto, *Phys. Rev. B* **70** (2004) 115112.
- ³⁰ A. Mishima, K. Nasu, *Phys. Rev. B* **39** (1989) 5763.
- ³¹ A. Mishima, K. Nasu, *Phys. Rev. B* **39** (1989) 5758.
- ³² H. Tanaka, S. Kuroda, T. Yamashita, M. Mitsumi, K. Toriumi, *J. Phys. Soc. Jpn.* **72** (2003) 2169.
- ³³ J. Ohara, S. Yamamoto, *Phys. Rev. B* **70** (2004) 115112.

This figure "Fig3.jpg" is available in "jpg" format from:

<http://arxiv.org/ps/cond-mat/0512635v1>